Bulk and surface properties of layered silicates/fluorinated polyimide nanocomposites

Liang-You Jiang and Kung-Hwa Wei

Citation: Journal of Applied Physics **92**, 6219 (2002); doi: 10.1063/1.1516268
View online: http://dx.doi.org/10.1063/1.1516268
View Table of Contents: http://scitation.aip.org/content/aip/journal/jap/92/10?ver=pdfcov
Published by the AIP Publishing

Bulk and surface properties of layered silicates/fluorinated polyimide nanocomposites

Liang-You Jiang and Kung-Hwa Wei[a)]
Department of Materials Science and Engineering, National Chiao Tung University, Hsinchu, Taiwan 30049, Republic of China

(Received 24 June 2002; accepted 29 August 2002)

Intercalated layered silicates/fluorinated polyimide nanocomposites with good overall properties are synthesized from organics-modified-montmorillonite and poly(amic acid), as confirmed by x-ray and transmission electron microscopy results. Both the bulk and surface (nanometer-domain) mechanical properties of synthesized silicates/fluorinated polyimide nanocomposites increased substantially as compared to that of pure polyimide. In particular, the Young's modulus and surface hardness of the fluorinated polyimide containing 5 wt % $2NH_2$-mont are 69% and 100% larger than that of pure polyimide, respectively. Additionally, the reduced elastic modulus by nanoindentation of the nanocomposites is 74% larger than that of the pure polyimide. The barrier properties of the nanocomposites, such as thermal expansion and water absorption retardation, are enhanced. © *2002 American Institute of Physics.* [DOI: 10.1063/1.1516268]

I. INTRODUCTION

Polyimides are high-performance materials possessing excellent thermal, mechanical and electricity-resistant properties. Consequently, they have been widely used in the aerospace, electrical, and microelectronics industries. Fluorinated polyimides in particular offer low dielectric constants and are suitable for the microelectronics industry. Owing to the presence of flexible hexafluoroisopropylidene groups, $-(CF_3)_2C-$, in the polymer chain, the coefficients of thermal expansion of the fluorinated polyimide are higher and the tensile mechanical properties are lower than that of the aromatic polyimides without fluorines.[1–4] Natural montmorillonite consists of stacks of disk-shaped silicate layers with a thickness of about 1 nm and a diameter ranging from 100 to 200 nm. With a high aspect ratio, high tensile modulus, and low thermal expansion, silicates are an ideal component for forming organic-inorganic hybrid materials. For example, layered silicates/polyimide nanocomposites[5–16] display reduced coefficients of thermal expansion, enhanced tensile-mechanical properties and retarded water absorption properties by having only a few weight percent of layered silicates dispersed in the nanometer scale in the polyimide matrix. As electronic devices shrink further in the pursuit of high performance, the surface properties of the polyimide thin films become very critical. The surface and elastic behavior of these layered silicates/polyimides, however, are rarely studied.

Nanoindentation experiments performed at very low loads and small penetration depths give the elastic behavior and surface hardness of thin film materials. The surface nanomechanical properties of polymer films can be quite different from that of the bulk material. Recently, the nanoindentation measurements of copolymer and polymer/inorganic conventional composites have been carried out. For example, the relationship between the surface elastic modulus and the hard-to-soft segment ratio of polyurethane is studied.[17] Additionally, the distribution of hardness in dry and water aged polyester/glass and phenolic/glass is investigated by nanoindentation.[18,19]

In our previous study,[15] the moisture barrier and current leakage properties of polyimide containing layered silicates, having dimensions of 1 nm×1200 nm, have been greatly improved, and therefore this type of polyimide nanocomposite is suitable for use as an advanced dielectric material in microelectronics applications. The surface properties of these nanocomposite films, which are very important in multilayer device applications, however, are not usually studied. In this study, layered silicates with dimensions 1 nm×200 nm are dispersed in polyimide, to obtain nanocomposites with smaller interfaces. The bulk and nanodomain surface mechanical properties, along with thermal and water-barrier properties, of these nanocomposites are investigated.

II. EXPERIMENTAL SECTION

A. Materials

Na^+ montmorillonite (PK-802), supplied by Pai Kong Industries, Taiwan, had a cation exchange capacity of 114 meq/100 g. 4,4′-(hexafluoroisopropylidene)-diphathalic anhydride (6FDA) was purchased from Chriskev. 4,4′-oxydianiline (ODA) and 2,2-bis[4-(4-aminophenoxy)phenyl] propane ($2NH_2$) were obtained from TCI in Tokoyo, Japan. *N*,*N*-Dimethylacetamide (DMAc) was obtained from Tedia in Ohio.

B. Preparation of organics-modified montmorillonite and nanocomposites

A solution of $2NH_2$, (2.1 g dissolved in 100 ml of 0.1 N HCl), was gradually added to a previously prepared solution of 10 g screened PK-802 in 1 L of de-ionized water. The mixture was vigorously stirred for 5 days at 25 °C. After-

a)Author to whom correspondence should be addressed; electronic mail: khwei@nctu.edu.tw

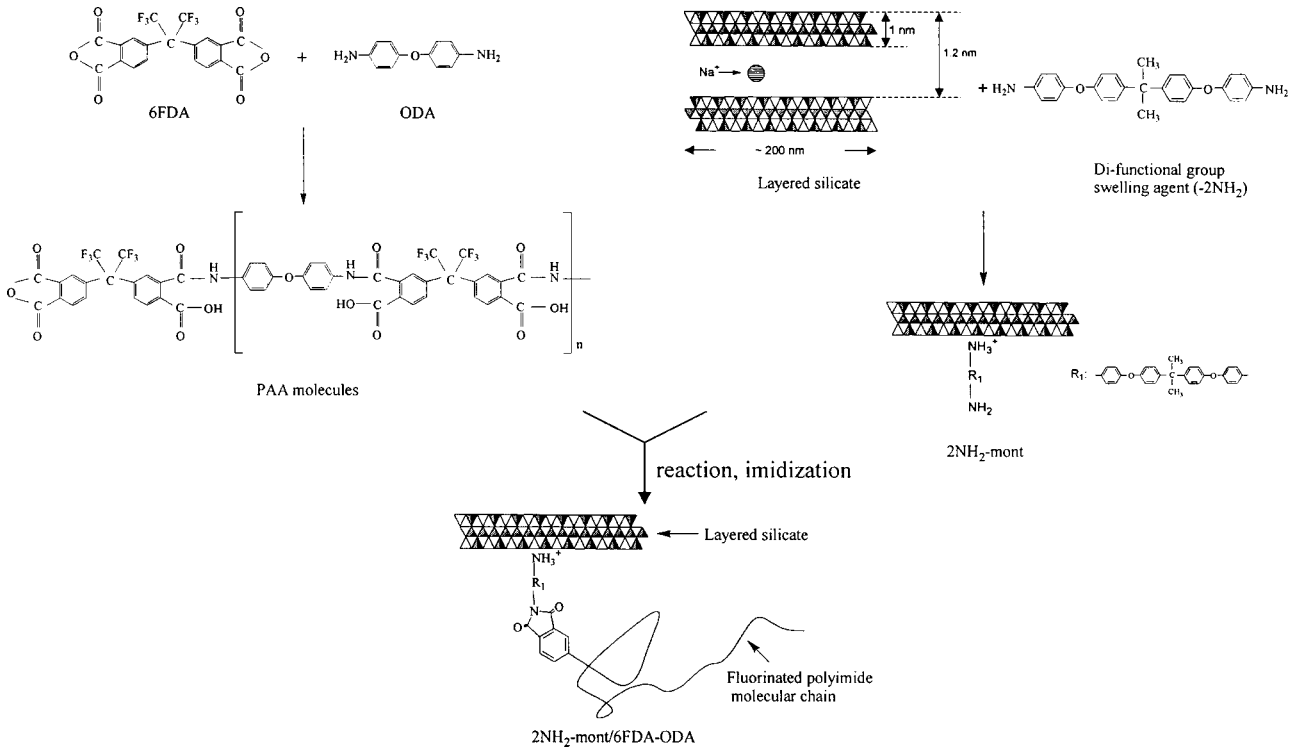

FIG. 1. Synthesis procedure of $2NH_2$-mont/6FDA–ODA nanocomposites from organics-modified montmorillonite and fluorinated polyimide.

wards, the suspension was repeatedly washed with deionized water. The filtrate was titrated with 0.1 N $AgNO_3$ until AgCl no longer precipitated, which ensured the complete removal of chloride ions. Then, the filter cake was placed in a vacuum oven at 120 °C for 1 day of drying. The powder obtained was termed $2NH_2$-mont.

Different concentrations of suspensions were prepared by putting 0.045, 0.09, 0.27, and 0.45 g of $2NH_2$-mont in 13.34 g DMAc, respectively, and by mixing each of them for 12 h. Poly(amic acid) was synthesized by putting 2.75 g of ODA into a three-neck flask containing 33.73 g DMAc under nitrogen purge at 25 °C. After ODA was completely dissolved in DMAc, 6.22 g of 6FDA, being divided into three batches, was added to the flask batch-by-batch with a time interval of 20 min between batches. After all the 6FDA was dissolved in DMAc containing ODA, the solution was mixed for about 20 min. A viscous poly(amic acid) solution was obtained. The previously prepared $2NH_2$-mont suspensions were added into the poly(amic acid) solution under mixing. The mixtures in the flask were stirred for 20 h, and the $2NH_2$-mont/poly(amic acid) solution was obtained. The final solid content of poly(amic acid) in DMAc is 16%.

The $2NH_2$-mont/poly(amic acid) nanocomposite films were prepared by casting the solution on glass plates by a doctor blade. The solvent in $2NH_2$-mont/poly(amic acid) solution was removed in a vacuum oven at 30 °C for 48 h before the imidization step. Imidization of $2NH_2$-mont/poly(amic acid) was carried out by putting the samples in an air-circulation oven at 100, 150, 200, and 300 °C for 1 h, respectively, and then at 350 °C for 30 min to ensure a complete imidization. The synthetic procedure of $2NH_2$-mont/6FDA–ODA is presented in Fig. 1.

C. Characterization

X-ray diffraction studies of the samples were carried out with MAC Science MXP18 x-ray diffractometer (30 kV, 20 mA) with a copper target at a scanning rate of 4°/min. The samples for the transmission electron microscopy (TEM) study was first prepared by putting $2NH_2$-mont/6FDA–ODA films into epoxy capsules and by curing the epoxy at 70 °C for 48 h in a vacuum oven. The cured epoxy samples were then microtomed with Leica Ultracut Uct into about 90-nm-thick slices for observation with TEM. The type of TEM used is JEOL JEM-1200EX II, with an acceleration voltage of 120 kV. In the nanoindentation experiments, the samples were prepared by spin-coating $2NH_2$-mont/poly(amic acid) solution onto a silicon substrate, followed by the same imidzation condition as described in the preceding paragraph. The thickness of the imidized $2NH_2$-mont/6FDA–ODA films was about 7 μm. A Berkovich indenter was used in the nanoindentation experiment, which is mounted on the indenter head and is a three-sided triangular-based pyramidal diamond (TI-039), made by Hysitron Inc., The cross section of the base of the Berkovich indenter is 6 μm$\times$6 μm. The maximum load is 1000 μN, the loading and unloading times are 20 s, respectively, and the waiting time is 5 s for the nanoindentation experiments. Each of the data points in the nanoindentation test was determined by five samples. The tensile properties of $2NH_2$-mont/6FDA–ODA films were measured according to the specifications of ASTM D882-88 at a crosshead speed of 2 mm/min with an Instron 5500R tester. The films were first heated to 160 °C under vacuum for 4 days to dry, and then the water absorption study was performed at 40 °C under 90% RH. Differences in the weight

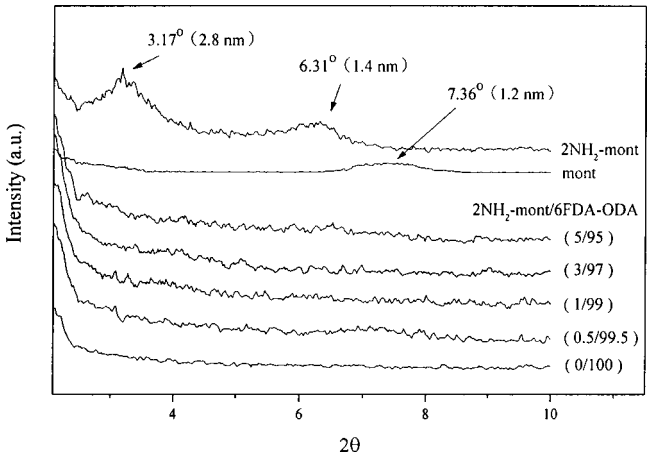

FIG. 2. X-ray diffraction curves of pure montmorillonite, $2NH_2$-mont and $2NH_2$-mont/6FDA–ODA films.

of the films were measured every 10 h. Measurements of the films' coefficients of thermal expansion (CTE) were carried out using a Du Pont TMA 2940 (film probe), which provided 0.05 N tensile force on the film at a heating rate of 10 °C/min in a nitrogen atmosphere.

III. RESULTS AND DISCUSSION

The x-ray diffraction curves of pure montmorillonite, $2NH_2$-mont and $2NH_2$-mont/6FDA–ODA are presented in Fig. 2. For the pure montmorillonite, the x-ray diffraction peak at $2\theta=7.4°$ is caused by the diffraction of the (001) crystal surface of layered silicates, equaling a d spacing of 1.2 nm. For $2NH_2$-mont, the diffraction peak at $2\theta=3.2°$ represents a d spacing of 2.8 nm in the silicate layers. Additionally, in Fig. 2, no x-ray diffraction peaks at $2\theta=3–10°$ appeared in the $2NH_2$-mont/6FDA–ODA films, indicating that the d spacings of the silicate layers in $2NH_2$-mont are larger than 3.0 nm. Figure 3 presents direct evidence of the nanometer-scale dispersion of intercalated silicate layers in 6FDA–ODA, as demonstrated in their TEM micrographs. In Fig. 3(a), for 1 wt % $2NH_2$-mont in 6FDA–ODA, silicate layers were clearly intercalated in some regions of the film with layer-to-layer distances ranging from 4 to 8 nm. As the amount of $2NH_2$-mont increases to 5 wt %, the dispersion of silicate layers in 6FDA–ODA both intercalates and aggregates in some regions, as shown in Fig. 3(b). Figure 3 also reveals the orientation of the silicate layers, as represented by the dark lines that have an inclination parallel to the surface direction of the nanocomposite films.

The tensile mechanical properties of these nanocomposites are given in Table I. The Young's modulus of 6FDA–ODA having 3 wt % $2NH_2$-mont was 35% higher than that of pure 6FDA–ODA (2.03 vs 1.51 GPa). The modulus of the nanocomposite further increases to 2.55 GPa at 5 wt % $2NH_2$-mont content, a 69% increase. The maximum stress also increases with the amount of $2NH_2$-mont. For 5 wt % $2NH_2$-mont in 6FDA–ODA, the maximum stress is 96.6 MPa, which is 37% higher than that of pure 6FDA–ODA (70.7 MPa). The elongation-for-break of $2NH_2$-mont/6FDA–ODA decreases only slightly with increasing amounts of $2NH_2$-mont. These results are attributed to the reinforcement of 6FDA–ODA by stiff layered silicates and the relatively good bonding between $2NH_2$-mont and 6FDA–ODA.

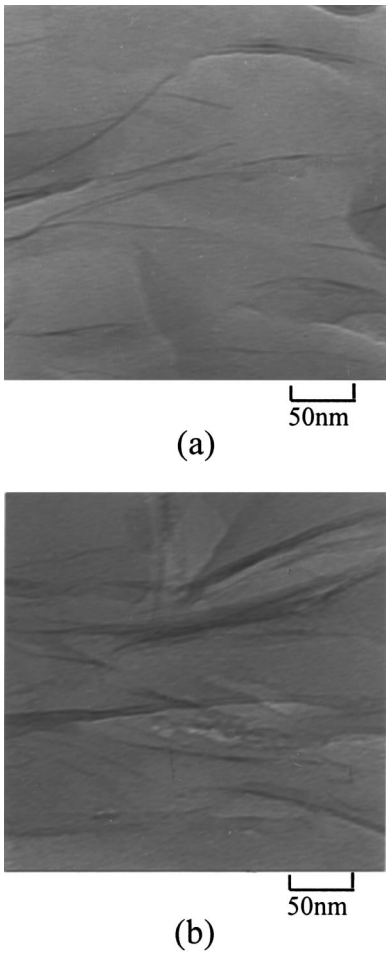

FIG. 3. Transmission electron microscopy micrographs of a cross-section view of $2NH_2$-mont/6FDA–ODA nanocomposite films containing (a) 1 wt % $2NH_2$-mont and (b) 5 wt % $2NH_2$-mont.

Figure 4 displays the schematics of the Berkovich indenter used in the experiment and an image of the indented nanocomposite surface after the nanoindentation experiment. Figure 5 gives a typical load-displacement curve, consisting of the loading and the unloading cycles for 1 wt % $2NH_2$-mont/6FDA–ODA nanocomposite. The initial slope of the unloading curve is used to calculate the stiffness of the sample as shown in the following equation:[18]

TABLE I. Tensile-mechanical properties of $2NH_2$-mont/6FDA–ODA nanocomposites containing different amounts of organomont.

Content of $2NH_2$-mont (wt %)	Modulus (GPa)	Max. stress (MPa)	Elongation (%)
0	1.51±0.03	70.7±2.0	18.3±1.6
0.5	1.73±0.06	77.8±3.4	10.7±0.5
1.0	1.90±0.02	86.8±1.6	11.0±0.5
3.0	2.03±0.01	89.8±3.0	11.5±0.4
5.0	2.55±0.12	96.6±3.7	7.7±0.7

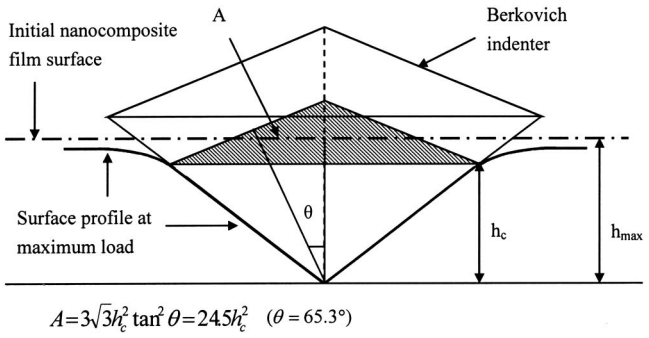

(a)

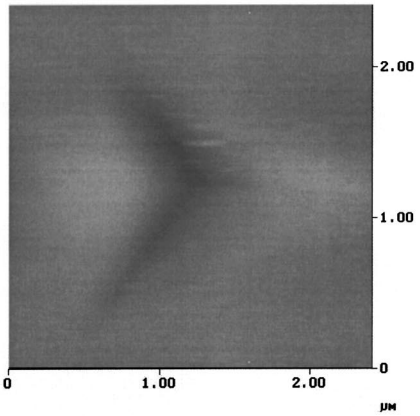

(b)

FIG. 4. (a) Schematic drawing of the side view of the Berkovich indenter, (b) the image of nanoindented 1 wt % $2NH_2$-mont/6FDA–ODA nanocomposite film after the experiment (top view).

$$S=\frac{dp}{dh}. \tag{1}$$

Here, P is the measured load, and h is the depth of penetration. The stiffness is used to calculate the hardness (H) and reduced elastic modulus (E_r). The hardness of the nanocomposite material measured by the Berkovich tip is given by the following equation:[18,19]

$$H=\frac{P}{A}=\frac{P}{24.5h_c^2}, \tag{2}$$

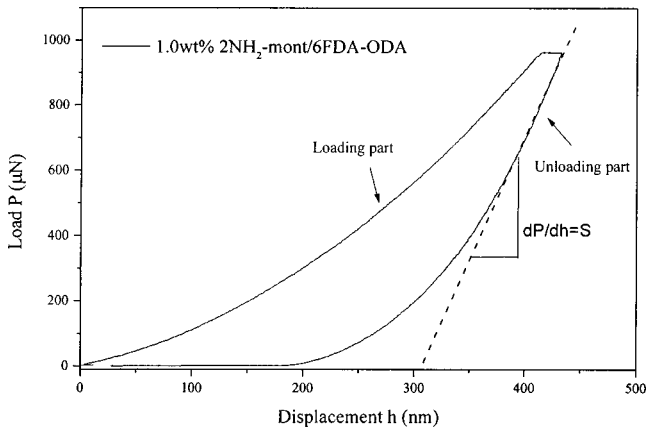

FIG. 5. Load and recovery displacement curve of the 1 wt % $2NH_2$-mont/6FDA–ODA nanocomposite for the nanoindentation test.

TABLE II. The surface nanomechanical properties of $2NH_2$-mont/6FDA–ODA nanocomposites by nanoindentation measurement.

Content of $2NH_2$-mont (wt %)	Reduced elastic modulus, E_r (GPa)	Surface hardness (GPa)	Max. displacement (nm)
0	3.1±0.1	0.17±0.02	500±13
0.5	3.6±0.1	0.22±0.01	435±6
1.0	3.9±0.1	0.25±0.02	415±6
3.0	4.5±0.1	0.28±0.02	403±4
5.0	5.4±0.2	0.34±0.01	372±7

where P is the load, A is the contact area ($A=24.5h_c^2$) as shown in Fig. 4(a) and h_c is the contact depth which is calculated with the following:[20]

$$h_c=h_{\max}-0.75\left(\frac{P_{\max}}{S}\right). \tag{3}$$

The reduced elastic modulus (E_r) is given by Eq. (4):[18–20]

$$E_r=\frac{\sqrt{\pi}S}{2\beta\sqrt{A}}, \tag{4}$$

where A is the contact area and $\beta=1.034$ for a triangular indenter.[20] Table II gives the surface nanomechanical properties of these nanocomposites. The reduced elastic modulus increases with the amount of $2NH_2$-mont. In particular, for 5 wt % $2NH_2$-mont in 6FDA–ODA, the reduced elastic modulus is 74% larger than that of pure 6FDA–ODA (5.4 vs 3.1 GPa), indicating that the presence of $2NH_2$-mont leads to greater surface elastic behavior. The surface hardness also increases with the amount of $2NH_2$-mont. When the amount of $2NH_2$-mont in 6FDA–ODA reaches 5 wt %, the hardness of the nanocomposite doubles (0.34 vs 0.17 GPa), and the resultant displacement is reduced by 26%. These results indicate that the orientation of the stiff layered silicates determines the near-surface properties of the nanocomposites.

The difference between bulk tensile-mechanical and nanoindentation properties can be demonstrated in Fig. 6. In Fig. 6, the orientation of the silicate layers is determined from TEM observation. In a bulk tensile-mechanical test, the direction of the tensile force is parallel to the surface of the nanocomposite film. The layered silicates act as stiffeners that enhance the Young's modulus and the tensile stress of polyimide nanocomposites due to the large and multiple in-

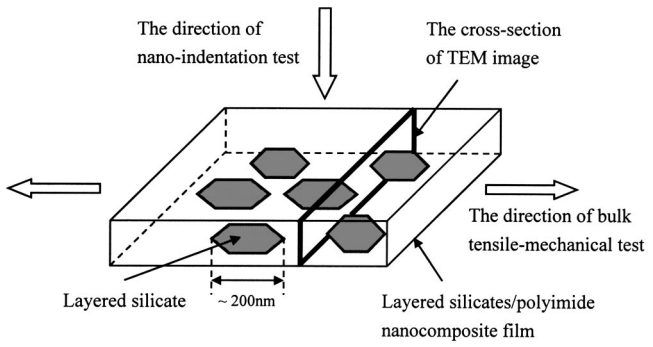

FIG. 6. Schematic drawing of the nanostructured layered silicates/polyimide film under various measurements.

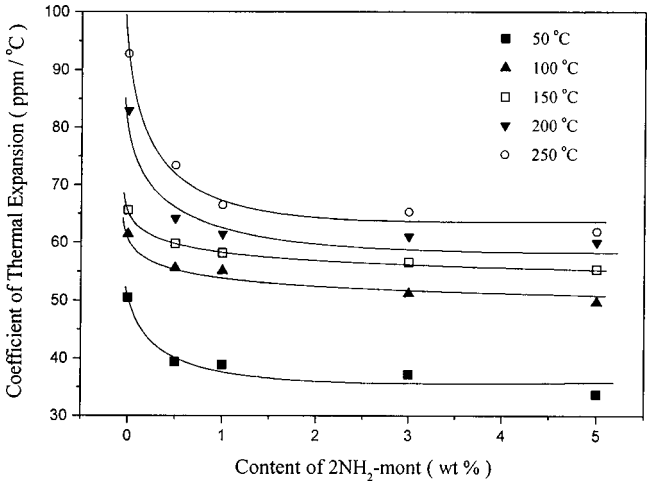

FIG. 7. Coefficients of thermal expansion of different compositions of $2NH_2$-mont/6FDA–ODA at different temperatures.

terfacial bonding between the silicates and polyimide. The direction of the indentation load is vertical to the surface in a nanoindentation experiment. The cross-sectional area of the silicates provides resistance to the indenting load. Therefore, the reduced elastic modulus and the surface hardness increases with adding $2NH_2$-mont in 6FDA–ODA.

The CTE of $2NH_2$-mont/6FDA–ODA at different temperatures is shown in Fig. 7. The CTE of $2NH_2$-mont/6FDA–ODA decreases dramatically at 1 wt % $2NH_2$-mont concentrations and levels off at 3 wt % $2NH_2$-mont concentrations. This phenomenon is due to the fact that as the amount of $2NH_2$-mont increases, the extent of dispersion of the layered silicates becomes poorer, and their total retardation on the thermal expansion of polyimide is reduced.

The evolution of water absorption in the $2NH_2$-mont/6FDA–ODA nanocomposite films under ambient conditions of 90% relative humidity and 40 °C are shown in Fig. 8. In Fig. 8, for the pristine 6FDA–ODA films, the saturated amount of absorbed water is 0.60% after 40 h. In the case of 6FDA–ODA films containing 3 wt % $2NH_2$-mont, the saturated amount of absorbed water is 0.27%, which is 55% lower than that of the pristine 6FDA–ODA. As explained in our previous study,[15] this behavior is due to polyimide intercalated in the galleries of the hydrophobic organic-modified layered silicates, which absorb almost no water. Hence, the equilibrium water absorption of $2NH_2$-mont/6FDA–ODA nanocomposite films decreases with the amount of $2NH_2$-mont. The equilibrium water absorption in the nanocomposites does not decrease monotonically with the increasing amount of silicates, but reaches a minimum value at 3 wt % silicate content. This behavior is explained by the fact that the dispersion of silicates in 6FDA–ODA becomes more aggregated, and the amount of 6FDA–ODA intercalated in the layered silicates is reduced as the silicate content exceeds 3 wt %.

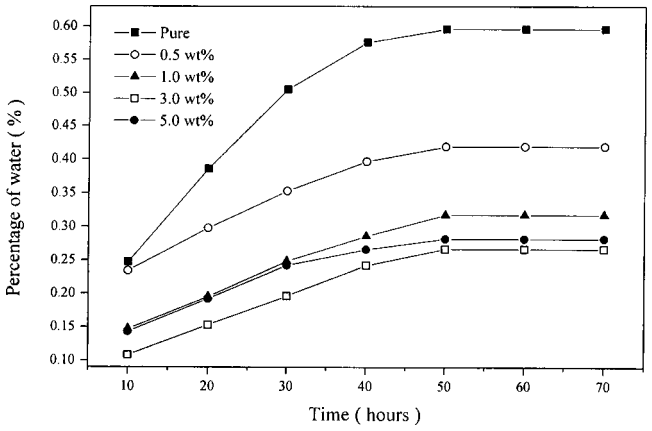

FIG. 8. Evolution of water absorption of $2NH_2$-mont/6FDA–ODA nanocomposites at different compositions.

IV. CONCLUSION

$2NH_2$-mont/6FDA–ODA nanocomposites with good overall properties were developed by reacting organics-modified montmorillonite and poly(amic acid). The presence of a small percentage of high-aspect-ratio, nanometer-sized layered silicates in the polyimide matrix lead to much better bulk and surface mechanical properties, reduced thermal expansion, and decreased water absorption, as compared to neat polyimide.

ACKNOWLEDGMENT

The authors appreciate the financial support provided by the National Science Council through Project No. NSC 90-2216-E-009-017.

[1] K. L. Mittall, *Polyimide: Synthesis Characterization and Application* (Plenum, New York, 1984).
[2] C. Feger, M. M. Khojastech, and J. E. McGrath, *Polyimide: Materials, Chemistry and Characterization* (Elsevier, Amsterdam, 1989).
[3] D. Wilson, H. D. Stenzenberger, and P. M. Hergenrother, *Polyimides* (Blackie, Glasgow, 1990).
[4] M. K. Ghosh and K. L. Mittal, *Polyimides, Fundamentals and Applications* (Marcel Dekker, New York, 1996).
[5] K. Yano, A. Usuki, A. Okada, T. Kurauchi, and O. Kamigaito, J. Polym. Sci., Part A: Polym. Chem. **31**, 2493 (1993).
[6] T. Lan, P. D. Kaviratna, and T. J. Pinnavaia, Chem. Mater. **6**, 573 (1994).
[7] K. Yano, A. Usuki, and A. Okada, J. Polym. Sci., Part A: Polym. Chem. **35**, 2289 (1997).
[8] Y. Yang, Z. K. Zhu, J. Yin, X. Y. Wang, and Z. E. Qi, Polymer **40**, 4407 (1999).
[9] J. C. Huang, Z. K. Zhu, X. D. Ma, X. F. Qian, and J. Yin, J. Mater. Sci. **36**, 871 (2001).
[10] H. L. Tyan, Y. C. Liu, and K. H. Wei, Chem. Mater. **11**, 1942 (1999).
[11] H. L. Tyan, C. Y. Wu, and K. H. Wei, J. Appl. Polym. Sci. **81**, 1742 (2001).
[12] H. L. Tyan, C. M. Leu, and K. H. Wei, Chem. Mater. **13**, 222 (2001).
[13] T. Agag, T. Koga, and T. Takeichi, Polymer **42**, 3399 (2001).
[14] D. M. Delozier, R. A. Orwoll, J. F. Cahoon, N. J. Johnston, J. G. Smith, Jr., and J. W. Connell, Polymer **43**, 813 (2002).
[15] L. Y. Jiang, C. M. Leu, and K. H. Wei, Adv. Mater. **14**, 426 (2002).
[16] C. M. Leu, Z. W. Wu, and K. H. Wei, Chem. Mater. **14**, 3016 (2002).
[17] E. Amitay-Sadovsky, B. Ward, G. A. Somorjai, and K. Komvopoulos, J. Appl. Phys. **91**, 375 (2002).
[18] A. Hodzic, Z. H. Stachurski, and J. K. Kim, Polymer **41**, 6895 (2000).
[19] A. Hodzic, J. K. Kim, and Z. H. Stachurski, Polymer **42**, 5701 (2001).
[20] B. Bhushan, *Handbook of Micro/Nanotribology*, CRC Press, Boca Raton, FL, 1995), Chap. 9.